

# Behaviour of dissipative accretion flows around black holes

Santabrata Das<sup>★</sup>

*Astrophysical Research Center for the Structure and Evolution of the Cosmos (ARCSEC), Sejong University, 98 Gunja-Dong, Gwangjin-Gu, Seoul 143-747, South Korea*

Accepted 2007 January 11. Received 2007 January 9; in original form 2006 August 25

## ABSTRACT

We investigate the behaviour of dissipative accreting matter close to a black hole, as this provides important observational features of galactic and extragalactic black hole candidates. We find a complete set of global solutions in the presence of viscosity and synchrotron cooling. We show that advective accretion flow can have a standing shock wave and the dynamics of the shock is controlled by the dissipation parameters (both viscosity and cooling). We study the effective region of the parameter space for standing as well as oscillating shock. We find that the shock front always moves towards the black hole as the dissipation parameters are increased. However, viscosity and cooling have opposite effects in deciding the solution topologies. We obtain two critical cooling parameters that separate the nature of the accretion solution.

**Key words:** accretion, accretion discs – black hole physics – shock waves.

## 1 INTRODUCTION

The process of accretion around compact objects has been extensively studied during last three decades. Several attempts have been made to develop a theory of accretion discs. The standard theory of thin accretion discs provides a self-consistent solution of the Keplerian disc model (Shakura & Sunyaev 1973, hereafter SS73). Soon after the standard disc model was proposed, it was realized that discs are not Keplerian everywhere, particularly in radiation pressure dominated regions (Lightman & Eardley 1974; Chakrabarti 1996a). In addition, this model (SS73) was not successful in explaining the origin of observed high-energy radiation. A possible solution was immediately proposed in the literature (Sunyaev & Titarchuk 1985); that is, a disc may possess a Compton cloud, which must inverse Comptonize the Keplerian soft photons to produce the hard X-rays. Incidentally, Chakrabarti & Molteni (1995) and Lanzafame, Molteni & Chakrabarti (1998) showed using numerical simulations that angular momentum distribution depends on the viscosity prescription under consideration and remains sub-Keplerian close to the black hole as flow must cross the horizon supersonically (Chakrabarti 1990). Recent observations do support the fact that sub-Keplerian matter may be present in accretion discs (Smith et al. 2001; Smith, Heindl & Swank 2002).

In earlier studies, Chakrabarti (1989, 1990) extensively discussed the transonic properties of inviscid, polytropic flows and showed that standing shock waves can form for a large region of parameter space spanned by the specific energy and specific angular momentum of the flow. Various authors (Nobuta & Hanawa 1994; Yang & Kafatos 1995; Lu & Yuan 1997; Fukumura & Tsuruta 2004; Gu & Lu 2004) found the existence of standing shock waves in different astrophys-

ical contexts. In an accretion process around a black hole, flow is subsonic at a large distance and crosses the horizon supersonically. Thus, black hole accretion is necessarily transonic. For a given set of input parameters, namely specific energy and specific angular momentum, the flow passes through the outer sonic point ( $x_{\text{out}}$ ) and remains supersonic as it proceeds inwards. At a distance  $x_s$  ( $< x_{\text{out}}$ ), flow is virtually stopped as a result of the resistance offered by the centrifugal barrier, and consequently a shock is formed. The post-shock flow momentarily becomes subsonic and flow temperature increases in this region as the kinetic energy of the flow is converted into thermal energy. Subsequently, flow picks up velocity as it approaches the black hole horizon and eventually crosses the horizon supersonically after passing through the inner sonic point ( $x_{\text{in}}$ ).

The first global and fully self-consistent solution of viscous transonic flows, including advection in the optically thin and thick limits, was obtained by Chakrabarti (1990,) and references therein. Here, it was assumed that Keplerian flow at the outer edge can become sub-Keplerian at the inner part of the disc. Later, Chakrabarti & Das (2004) presented a complete classification of global solutions of viscous transonic flow according to solution topologies, and identified the region in the parameter space where the flow possesses multiple sonic points. Within this region, if the viscosity parameter is below its critical value ( $\alpha_{\text{T}} < \alpha_{\text{T,s}}$ ), there are solutions where Rankine–Hugoniot shock conditions (RHCs; Landau & Lifshitz 1959) are satisfied and a standing shock is formed as a result of the centrifugal barrier (Chakrabarti 1990, 1996b; Chakrabarti & Das 2004). When viscosity is increased beyond a critical value, shocks disappear (see fig. 12 of Chakrabarti & Das 2004). Of course, the viscosity parameter depends greatly on model parameters such as the sonic point location and the angular momentum at the inner boundary. The importance of critical viscosity is being reconsidered by Gu & Lu (2004), where a ‘qualitative’ estimate of critical viscosity for standing shock ( $\alpha_{\text{T,s}} \leq 0.5$ ) has been reported. Furthermore, many authors

<sup>★</sup>E-mail: sbdas@canopus.cnu.ac.kr

have pointed out that shocks may undergo radial, vertical or non-axisymmetrical oscillations (Molteni, Toth & Kuznetsov 1999; Gu & Foglizzo 2003), although they are generally never ruined by these oscillations. In Das & Chakrabarti (2004), bremsstrahlung cooling was also added, bearing in mind that it is a very inefficient cooling process (Chattopadhyay & Chakrabarti 2000), and a complete set of global solutions of viscous transonic flow with and without shocks was presented. The hot and dense post-shock flow, which basically acts as a ‘boundary layer’ for the black holes, could be the natural site of hot radiation in accretion discs. This is considered to be a powerful tool for understanding important astrophysical phenomena such as the spectral properties of black holes (Chakrabarti & Titarchuk 1995; Chakrabarti et al. 1996; Ebisawa, Titarchuk & Chakrabarti 1996; Mandal & Chakrabarti 2005), the source of quasi-periodic oscillation (QPO) of hard X-rays from black hole candidates (Molteni, Sponholz & Chakrabarti 1996; Ryu, Chakrabarti & Molteni 1997; Chakrabarti, Acharyya & Molteni 2004) and the generation of accretion-powered relativistic bipolar outflows/jets (Das et al. 2001a, and references therein). Recently, Chakrabarti & Mandal (2006) reported that this boundary layer could be responsible for the spectral state transition in at least some black hole candidates, such as Cyg X1. Also, Fender et al. (2000) and Dhawan, Mirabel & Rodriguez (2000) showed that outflow could be produced from the same region that emits Comptonized photons. A globally complete inflow–outflow solution of viscous accretion flow has also been found by Chattopadhyay & Das (2007).

Motivated by the above arguments, in this paper we wish to study stationary, axisymmetric, viscous accretion solutions around a Schwarzschild black hole in the presence of synchrotron cooling. Such dissipative viscous accreting flow has not yet been explored in the literature. The space–time geometry around a non-rotating black hole is satisfactorily described by the pseudo-Newtonian potential (Paczyński & Wiita 1980). We consider a similar viscosity prescription as in Chakrabarti (1996b). We calculate all relevant dynamical and thermodynamical flow variables and study in depth the dependence of such variables on flow parameters, such as specific energy, specific angular momentum and dissipation parameters (synchrotron cooling and/or viscosity parameters). We identify the solution topologies that are essential for shock formation. In the present study, we concentrate on a non-dissipative shock that preserves the energy across it. In a generalized accretion flow, cooling reduces the energy of the flow while viscosity not only tends to heat the flow but also lowers the flow angular momentum as flow accretes. Thus, the effects of viscosity and synchrotron cooling on the dynamical structure of the accretion flow are expected to be different. Because shock has observational consequences as mentioned above, it is therefore pertinent to know how the dynamics of shock is controlled by the dissipation parameters, in particular, whether the shock front moves inwards or outwards if the dissipation is increased. In this paper, we attempt to discuss this issue in depth. Moreover, we find that shock waves, standing or oscillating, are still formed even when at a very high dissipation limit. In this paper, we provide a useful formalism to study dissipative transonic accretion flow, which is independent of the black hole mass and valid for a wide range of accretion rates.

In Section 2, we present the governing equations, and in Section 3, we perform sonic point analysis. In Section 4, we study the global solution topologies and classify the parameter space for solutions having multiple sonic points as a function of cooling parameter. In Section 5, we study the dynamics of shock and the dependence of shock properties on the flow parameters. In Section 6, we classify the parameter space as a function of the cooling parameter in terms

of whether shocks, standing or oscillating, will form or not. In Section 7, we quantify the critical cooling parameters, and finally, in Section 8, we provide concluding remarks.

## 2 BASIC HYDRODYNAMIC EQUATIONS

We begin with a stationary, thin, viscous, axisymmetric accretion flow on to a Schwarzschild black hole. In this paper, we consider the pseudo-Newtonian potential introduced by Paczyński & Wiita (1980) to solve the problem, instead of using full general relativity. This allows us to use the Newtonian concept, while at the same time retaining all the salient features of the space–time geometry around a non-rotating black hole. The governing equations for the accreting flow are written on the equatorial plane of the accretion disc. The flow equations are made dimensionless by considering the units of length, time and mass as  $r_g = 2GM_{\text{BH}}/c^2$ ,  $2GM_{\text{BH}}/c^3$  and  $M_{\text{BH}}$ , respectively, where  $G$  is the gravitational constant,  $M_{\text{BH}}$  is the mass of the black hole and  $c$  is the velocity of light. Henceforth, all flow variables are expressed in geometrical units.

In the steady state, the hydrodynamics of the axisymmetric accreting matter around a non-rotating black hole in the pseudo-Newtonian limit is given by (Chakrabarti 1996b):

(i) the radial momentum equation

$$\vartheta \frac{d\vartheta}{dx} + \frac{1}{\rho} \frac{dP}{dx} - \frac{\lambda^2}{x^3} + \phi(x) = 0; \quad (1)$$

(ii) the mass flux conservation equation

$$\dot{M} = \Sigma \vartheta x; \quad (2)$$

(iii) the angular momentum conservation equation

$$\vartheta \frac{d\lambda(x)}{dx} + \frac{1}{\Sigma x} \frac{d}{dx} (x^2 W_{x\phi}) = 0; \quad (3)$$

(iv) the entropy generation equation

$$\Sigma \vartheta T \frac{ds}{dx} = \frac{h\vartheta}{\gamma - 1} \left( \frac{dP}{dx} - \frac{\gamma P}{\rho} \frac{d\rho}{dx} \right) = Q^+ - Q^-. \quad (4)$$

The local variables  $x$ ,  $\vartheta$ ,  $\rho$ ,  $P$  and  $\lambda$  in the above equations are the radial distance, radial velocity, density, isotropic pressure and angular momentum of the flow, respectively. Here,  $\phi(x) = -(1/2)(x - 1)^{-1}$  denotes the pseudo-Newtonian potential and  $\gamma$  is the adiabatic index of the flow. Furthermore,  $s$  and  $T$  are the specific entropy and the local temperature of the flow, respectively,  $\Sigma$  is the vertically integrated density and  $W_{x\phi}$  is the viscous stress. Here,  $Q^+$  and  $Q^-$  represent the energy gained and lost by the flow, respectively, and  $\dot{M}$  is the mass accretion rate. In our model, the accreting flow is assumed to be in hydrostatic equilibrium in the vertical direction. The half thickness of the disc is then obtained by equating the vertical component of the gravitational force and the pressure gradient force as

$$h(x) = ax^{1/2}(x - 1), \quad (5)$$

where  $a$  denotes the adiabatic sound speed defined as  $a = \sqrt{\gamma P/\rho}$ . In this paper, we use the similar viscosity prescription of Chakrabarti (1996b). In this prescription, viscous stress remains continuous across the axisymmetric shock wave for flows with significant radial motion.

Now we simplify the entropy equation (equation 4) as

$$\frac{\vartheta}{\gamma - 1} \left[ \frac{1}{\rho} \frac{dP}{dx} - \frac{\gamma P}{\rho^2} \frac{d\rho}{dx} \right] = \frac{Q^- - Q^+}{\rho h} = \Lambda - \Gamma. \quad (4a)$$

Here,  $\Gamma (= Q^+/\rho h)$  denotes the energy gained as a result of viscous heating and is obtained as

$$\Gamma = \frac{-\alpha_{\Pi} I_n x}{\gamma} (g a^2 + \gamma \vartheta^2) \frac{d\Omega}{dx}. \quad (6)$$

Here,  $\alpha_{\Pi}$  is the viscosity parameter and  $\Omega(x)$  is the angular velocity of the accreting matter at a radial distance  $x$ . The polytropic index is denoted by  $n = (1 - \gamma)^{-1}$ .  $I_n$  and  $I_{n+1}$  come from the vertically averaged density and pressure (Matsumoto et al. 1984) and  $g = I_{n+1}/I_n$ . The term  $\Lambda (= Q^-/\rho h)$  represents the energy loss by the flow. In the present analysis, we ignore energy loss due to bremsstrahlung cooling as it is not a very efficient cooling process (Chattopadhyay & Chakrabarti 2000), and we include synchrotron cooling only. Indeed, the magnetic field is ubiquitous inside the accretion disc and therefore the ionized flow in turn should emit synchrotron radiation that may cool down the accreting flow significantly. As the satisfactory description of the magnetic field inside the accretion disc is not well understood, we thus assume only a random or stochastic magnetic field. Such a magnetic field may or may not be in equipartition with the accretion flow. We define a parameter  $\eta$  as the ratio of the magnetic pressure and the thermal pressure of the flow under consideration, which is given by

$$\eta = \frac{B^2 \mu m_p}{8\pi \rho k_B T_p}. \quad (7)$$

Here,  $B$  denotes the magnetic field strength,  $k_B$  is the Boltzmann constant,  $\mu$  is the mean molecular weight and  $m_p$  is the mass of the proton. In general,  $\eta \lesssim 1$ , which ensures that magnetic fields definitely remain confined within the disc (Mandal & Chakrabarti 2005). While obtaining equation (7), we consider that the gas is assumed to obey an ideal equation of state. In an electron–proton plasma, we use an equipartition magnetic field (equation 7) to account for the non-dimensional synchrotron cooling effect, which is obtained in a convenient form as (Shapiro & Teukolsky 1983)

$$\Lambda = \frac{S a^5}{\vartheta x^{3/2} (x-1)}, \quad (8)$$

with

$$S = 7.5424 \times 1.44 \times 10^{17} \frac{\eta \beta \dot{m} \mu^2 e^4}{m_e^3 \gamma^{5/2}} \frac{1}{2G M_{\odot} c^3}. \quad (9)$$

Here,  $e$  and  $m_e$  represent the charge and mass of the electron, respectively. We estimate the electron temperature from the expression  $T_e = \sqrt{m_e/m_p} T_p$  (Chattopadhyay & Chakrabarti 2002) and use it to obtain equation (8). Here,  $\beta$  is a dimensionless cooling parameter that controls the efficiency of cooling. When  $\beta \rightarrow 0$ , the flow is heating dominated as it cools most inefficiently. In the present paper, we consider  $\gamma = 4/3$ ,  $\eta = 0.1$  and the accretion rate ( $\dot{m}$ ) = 0.233 (in units of Eddington rate), until otherwise stated.

### 3 SONIC POINT ANALYSIS

We solve equations (1)–(3) and (4a) following the standard method of sonic point analysis (Chakrabarti 1989). We calculate the radial velocity gradient as

$$\frac{d\vartheta}{dx} = \frac{N}{D}, \quad (10)$$

where the numerator  $N$  is given by

$$\begin{aligned} N = & \frac{S a^5}{x^{3/2} (x-1)} + \frac{\alpha_{\Pi}^2 I_n (a^2 g + \gamma \vartheta^2)^2}{\gamma^2 x} \\ & + \frac{\alpha_{\Pi}^2 g I_n a^2 (5x-3)(a^2 g + \gamma \vartheta^2)}{\gamma^2 x (x-1)} - \left[ \frac{\lambda^2}{x^3} - \frac{1}{2(x-1)^2} \right] \\ & \times \left[ \frac{(\gamma+1)\vartheta^2}{(\gamma-1)} - \frac{2\alpha_{\Pi}^2 g I_n (a^2 g + \gamma \vartheta^2)}{\gamma} \right] \\ & - \frac{\vartheta^2 a^2 (5x-3)}{x(\gamma-1)(x-1)} - \frac{2\lambda \alpha_{\Pi} I_n \vartheta (a^2 g + \gamma \vartheta^2)}{\gamma x^2} \end{aligned} \quad (10a)$$

and the denominator  $D$  is

$$\begin{aligned} D = & \frac{2a^2 \vartheta}{(\gamma-1)} - \frac{(\gamma+1)\vartheta^3}{(\gamma-1)} + \frac{\alpha_{\Pi}^2 I_n \vartheta (a^2 g + \gamma \vartheta^2)}{\gamma} \\ & \times \left[ 2g - 1 - \frac{a^2 g}{\gamma \vartheta^2} \right]. \end{aligned} \quad (10b)$$

The gradient of sound speed is obtained as

$$\frac{da}{dx} = \left( \frac{a}{\vartheta} - \frac{\gamma \vartheta}{a} \right) \frac{d\vartheta}{dx} + \frac{\gamma}{a} \left[ \frac{\lambda^2}{x^3} - \frac{1}{2(x-1)^2} \right] + \frac{(5x-3)a}{2x(x-1)} \quad (11)$$

and similarly, the gradient of angular momentum is calculated as

$$\frac{d\lambda}{dx} = \frac{\alpha_{\Pi} (a^2 g + \gamma \vartheta^2)}{\gamma \vartheta} - \frac{\alpha_{\Pi} x (a^2 g - \gamma \vartheta^2)}{\gamma \vartheta^2} \frac{d\vartheta}{dx} + \frac{2\alpha_{\Pi} a x g}{\gamma \vartheta} \frac{da}{dx}. \quad (12)$$

At the outer edge of the accretion disc, matter starts to accrete with almost negligible radial velocity and enters into the black hole with the velocity of light. This indicates that the ‘radial velocity gradient’ should be always real and finite to maintain the accretion flow smoothly along the streamline. However, equation (10b) indicates that there may be some points where the denominator ( $D$ ) vanishes. Because the flow is smooth everywhere along the streamline, at the point where the denominator tends to zero, the numerator ( $N$ ) must also vanish there. The point where both the numerator and denominator vanish simultaneously is called the critical point, or sonic point. Setting  $D = 0$ , we can easily obtain the expression for the Mach number ( $M = \vartheta/a$ ) at the sonic point as

$$M(x_c) = \sqrt{\frac{-m_2 - \sqrt{m_2^2 - 4m_1 m_3}}{2m_1}}, \quad (13)$$

where

$$m_1 = \gamma^2 \left[ \alpha_{\Pi}^2 I_n (2g-1)(\gamma-1) - (\gamma+1) \right]$$

$$m_2 = 2\gamma \left[ \gamma + \alpha_{\Pi}^2 I_n g (g-1)(\gamma-1) \right]$$

$$m_3 = -\alpha_{\Pi}^2 I_n g^2 (\gamma-1).$$

In the weak viscosity limit, the Mach number at the sonic point becomes

$$M(x_c) = \sqrt{\frac{2}{\gamma+1}}. \quad (13a)$$

This result is exactly the same as in Chakrabarti (1989). This indicates that the Mach number at the sonic point in the presence of different cooling processes remains the same as in the case for non-dissipative accretion flow. We obtain an algebraic equation for

sound speed by using another sonic point condition  $N = 0$ , which is given by

$$F(\mathcal{E}_c, \lambda_c, x_c) = \mathcal{A}a^3(x) + \mathcal{B}a^2(x) + \mathcal{C}a(x) + \mathcal{D} = 0, \quad (14)$$

where

$$\mathcal{A} = \frac{S}{x^{3/2}(x-1)}, \quad (14a)$$

$$\mathcal{B} = \left[ \frac{\alpha_{\Pi}^2 I_n (g + \gamma M^2)^2}{\gamma^2 x} + \frac{\alpha_{\Pi}^2 I_n g (5x - 3)(g + \gamma M^2)}{\gamma^2 x (x - 1)} - \frac{M^2 (5x - 3)}{x(\gamma - 1)(x - 1)} \right], \quad (14b)$$

$$\mathcal{C} = -\frac{2\lambda\alpha_{\Pi} I_n M (g + \gamma M^2)}{\gamma x^2}, \quad (14c)$$

and

$$\mathcal{D} = -\left[ \frac{\lambda^2}{x^3} - \frac{1}{2(x-1)^2} \right] \times \left[ \frac{(\gamma + 1)M^2}{(\gamma - 1)} - \frac{2\alpha_{\Pi}^2 g I_n (g + \gamma M^2)}{\gamma} \right]. \quad (14d)$$

We solve equation (14) analytically (Abramowitz & Stegun 1970) and obtain the sound speed at the sonic point by knowing the flow parameters. Depending on the input parameters, a non-dissipative flow may have a maximum of four sonic points (Das, Chattopadhyay & Chakrabarti 2001b). Among these, one always lies inside the horizon and the others, if they exist at all, remain outside the horizon. In our present analysis, we continue to use a similar concept to obtain dissipative accretion solutions (Chakrabarti & Das 2004). The nature of sonic points and their detailed properties can be easily understood with an extensive study of equation (10) when the flow parameters are known. In fact, the nature of sonic points depends on the value of velocity gradients at the sonic point (Ferrari et al. 1985; Muchotrzeb-Czerny 1986; Abramowicz & Kato 1989; Afshordi & Paczyński 2003; Chaudhury, Ray & Das 2006). In general,  $d\vartheta/dx$  possesses two values at the sonic point: one is for accretion flow and the other is valid for wind. When both the derivatives are real and of opposite signs, the sonic point is the saddle-type or X-type. A nodal-type sonic point is obtained when both the derivatives are real and of same sign. If the derivatives are complex, the sonic point belongs to the class of spiral-type or O-type. In the astrophysical context, the saddle-type sonic point has some special importance as transonic flows usually pass through it. In addition, in order to form a standing shock, the flow must have more than one saddle-type sonic point, among them the closest and furthest values corresponding to the inner and outer X-type sonic points. The O-type sonic point,

which lies between the two saddle-type sonic points, is non-physical in the sense that no stationary solution passes through it.

## 4 SOLUTION TOPOLOGIES

To obtain a complete solution, it is necessary to supply the boundary values of energy, accretion rate and angular momentum of the flow for a given viscosity ( $\alpha_{\Pi}$ ) and cooling parameter ( $\beta$ ) and to integrate equations (10)–(12) simultaneously with the help of equations (10a) and (10b). As the black hole solution is necessarily transonic, the flow must pass through the sonic points. In addition, the flow presumably originates from the Keplerian disc ( $x_{\text{Kep}}$ ) and it must carry angular momentum  $\lambda(x_{\text{Kep}})$ , a part of which is transported as a result of viscosity outwards, and the other part is advected into the black hole through the sonic point. The distribution of the angular momentum from the inner edge of the disc to  $x_{\text{Kep}}$  is obtained from equation (12). Incidentally, the acceptable range of angular momentum at the inner edge of the disc and the inner sonic point location of the accreting solution is very small (i.e.  $1.5 \lesssim \lambda_{\text{in}} \lesssim 2$  and  $2 \lesssim x_{\text{in}} \lesssim 4$ ; Chakrabarti 1989; Chakrabarti & Das 2004). Thus, we choose the inner sonic point location  $x_{\text{in}}$  and the angular momentum at the inner sonic point  $\lambda(x_{\text{in}})$  (hereafter, we denote this as  $\lambda_{\text{in}}$ ) as input parameters instead of the aforementioned energy and the angular momentum flow at the outer edge of the disc. We integrate once equations (10)–(12) inwards up to the horizon and again outwards to a large distance ( $\sim x_{\text{Kep}}$ ) to obtain a complete transonic solution. A comprehensive study of viscous transonic flow has already been presented by Chakrabarti & Das (2004) and therefore, in the current paper, we mainly concentrate on the properties of the accreting solution in the presence of synchrotron cooling, until otherwise stated.

### 4.1 Behaviour of global solutions

In order to obtain a shock solution around a black hole, the accreting flow must possess multiple saddle-type sonic points. The shock joins different solution branches, one passing through the inner sonic point and the other passing through the outer sonic point. Thus, it is important to understand the nature of solution trajectories in the presence of energy dissipation.

Fig. 1 shows examples of global solutions of inviscid accretion flow passing through the inner sonic point. Each box depicts Mach number ( $M = \vartheta/a$ ) variation as a function of the logarithmic radial distance. The cooling parameter  $\beta$  is marked in each box (0.0, 0.05, 0.1 and 0.2). The other flow parameters for Fig. 1 are chosen as  $x_c = 3.107$ ,  $\lambda_{\text{in}} = 1.6$  and  $n = 3$ . Here, all the sonic points are saddle-type, and the solutions may or may not have shock, depending on the global solution topologies. In the first column, the flow is free of dissipation and the sonic points are uniquely determined,

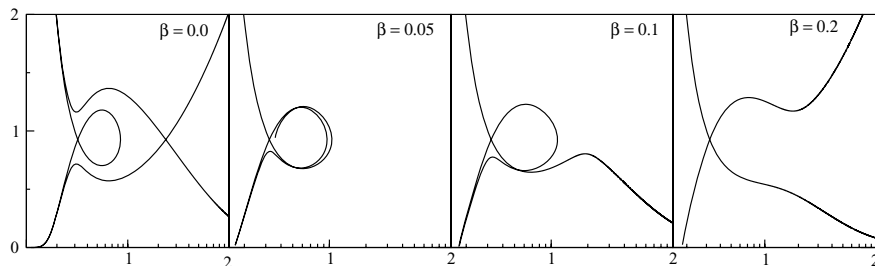


**Figure 1.** Global solution topologies in the presence of synchrotron cooling. In each box, the variation of the Mach number is plotted with logarithmic radial distance. Flow parameters are  $x_{\text{in}} = 3.107$  and  $\lambda_{\text{in}} = 1.6$ . Cooling parameters are marked in the figure.

as energy and angular momentum are conserved throughout. Accreting solutions of this type deviate from the Keplerian disc at the outer part of the disc and enter the black hole supersonically, with the radial velocity equal to the velocity of light after crossing the outer sonic point. Another possibility is that the supersonic flow may suffer shock transition at the subsonic branch, if shock conditions hold (see Section 5) and cross the black hole horizon after passing through the inner sonic point, as it has to satisfy the ‘supersonic’ inner boundary condition at the horizon. In the second column, cooling is incorporated and the flow topologies passing through the inner sonic point start to open up. The outer sonic point, if it exists, cannot be determined unless a shock is formed, as the energy of the flow is not conserved here. When cooling is increased further, the flow topologies are completely opened up (third and fourth columns) and they leave the accretion shock regime. In this particular situation, the flow deviates from the Keplerian disc far away from the black hole and enters it immediately through the inner sonic point. So, for a given set of flow parameters, there must be a critical cooling parameter ( $\beta_{cc}$ ) for which closed topologies passing through the same inner sonic point become open topologies. An exhaustive discussion of the critical cooling parameter is presented in Section 7.

#### 4.2 Description of the parameter space

In order to understand the dissipative accretion flow, here we classify the parameter space as a function of the cooling parameter in the  $\mathcal{E}_{in}-\lambda_{in}$  plane where  $\mathcal{E}_{in}$  denotes the energy of the flow at the inner sonic point ( $x_{in}$ ). In fact, in a cooling dominated inviscid accretion flow, the angular momentum remains conserved along the streamline of the flow. In Fig. 2, we have identified the region of the parameter space for the closed spiraling accretion solution, which

passes through the inner sonic point as in the first two boxes of Fig. 1. Accretion flows of this type possess multiple sonic points and flow may suffer shock transition if the outer sonic point exists. The shock would be stationary or oscillating depending on whether the Rankine–Hugoniot relation is satisfied or not. The region bounded by the solid curve is obtained for dissipation-free ( $\beta = 0$ ) accretion flow and it coincides with the result of Chakrabarti (1989). The dotted, dashed and dot-dashed regions are obtained for cooling parameters  $\beta = 0.00787$ ,  $0.0787$  and  $0.393$ , respectively. For higher  $\beta$ , the parameter space for closed topologies passing through the inner sonic point reduces in both lower and higher angular momentum sides. This is not surprising, as an increase of cooling induces damping inside the flow, which reduces the number of sonic points for the same set of initial parameters as seen in Fig. 1. With the rise of  $\beta$ , the effective region of parameter space for the closed topologies gradually shrinks and disappears completely when the critical cooling ( $\beta_{cc}$ ) is reached.

#### 5 SHOCK SOLUTIONS AND CLASSIFICATION OF PARAMETER SPACE

The existence of shock waves in accretion flow has been reported in many astrophysical contexts and the thermodynamical properties of shock waves, such as its location, strength and compression ratio, can be determined exactly by using RHCs. In the present study, we continue to use a similar viscosity prescription as in Chakrabarti (1996b), which keeps viscous stress ( $W_{x\phi}$ ) continuous across the shock in the presence of significant radial motion. We compute the shock locations following a useful technique first presented by Chakrabarti & Das (2004) for dissipative accretion flows.

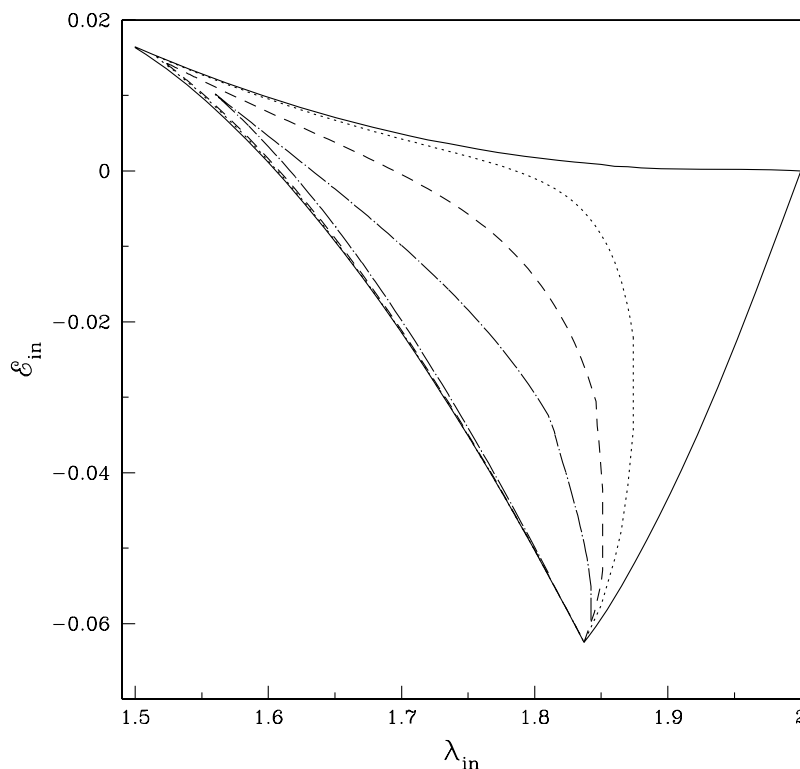


**Figure 2.** Classification of parameter space for closed topologies passing through the inner sonic point. The region bounded by different curves is obtained by using different cooling factors:  $\beta = 0.0$  (solid),  $\beta = 0.00787$  (dotted),  $\beta = 0.0787$  (dashed) and  $\beta = 0.393$  (dot-dashed). Note that the parameter space gradually shrinks with the increase of the cooling factor.

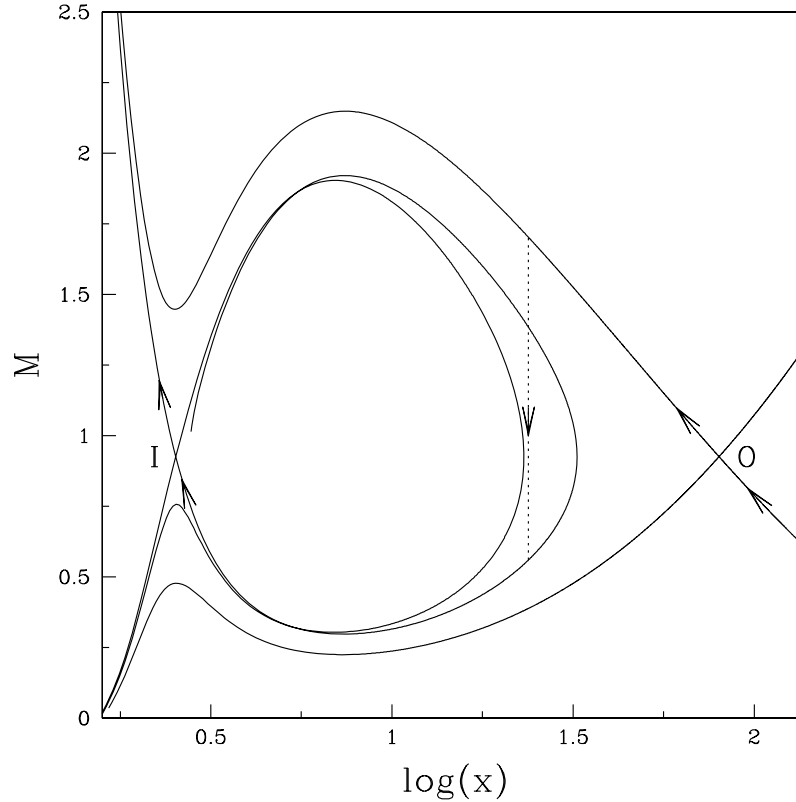


**Figure 3.** A complete accretion solution topology drawn with standing shocks ( $x_s = 23.83$ ). See text for details.

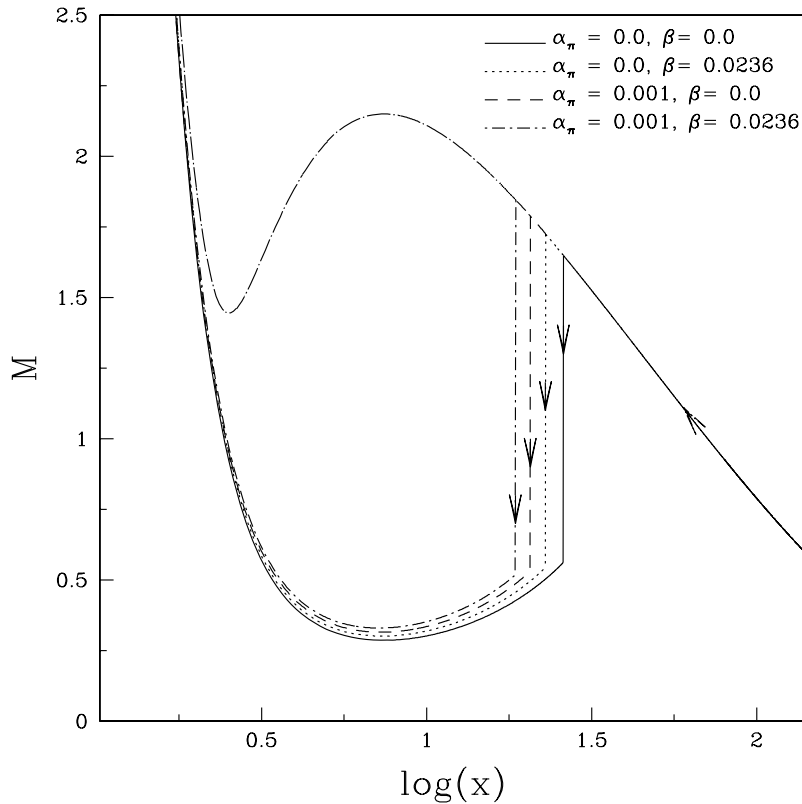
### 5.1 Shock dynamics and shock properties

Fig. 3 shows a complete solution of vertically averaged flow, where a shock wave connects two solution branches, one passing through the outer sonic point (O) and the other passing through the inner sonic point (I). In this figure, we plot the Mach number variation with the logarithmic radial distance. The flow parameters are chosen as  $x_{in} = 2.5308$ ,  $\lambda_{in} = 1.725$  and  $\beta = 0.0157$ , respectively. Subsonic accretion flow crosses the outer sonic point at  $x_{out} = 80.07$  and makes discontinuous transition (*shock*) at  $x_s = 23.82$  before entering into the black hole. The shock location is shown by the vertical dotted line. The exact location of the shock is obtained by solving Rankine–Hugotnot relations. In the present study, shock is assumed to be thin and non-dissipative. In addition, we ignore the presence of any excess sources of torque at the shock, which maintains the continuity of angular momentum across it. At the shock, entropy is generated, which is subsequently advected into the black hole.

Fig. 4 shows how the shock location (indicated by the vertical lines) changes with the dissipation parameters ( $\alpha_{\Gamma}$  and/or  $\beta$ ) for a given set of initial flow parameters. We inject matter subsonically at the outer edge of the disc  $x_{inj} = 145$  with local energy  $\mathcal{E}(x_{inj}) = 3.3663 \times 10^{-3}$  and angular momentum  $\lambda(x_{inj}) = 1.725$ . (Hereafter, we denote these as  $\mathcal{E}_{inj}$  and  $\lambda_{inj}$ , respectively.) The subsonic flow first passes through the outer sonic point and becomes supersonic. The RHCs are satisfied here and eventually a shock is formed. The solid vertical line represents the shock location ( $x_s = 25.99$ ) for non-dissipation ( $\alpha_{\Gamma} = 0$  and  $\beta = 0$ ) flow. As viscosity is turned on, the shock front ( $x_s = 20.6$ ) moves forward, denoted by the dashed vertical line. Because of viscosity, accreting flow loses angular momentum, causing the reduction of centrifugal pressure, and at the same time the energy of the flow increases. At the shock,

total pressure must be continuous and thus the dynamics of the shock are mainly controlled by the resultant pressure across it. As the shock moves in and as  $\lambda(x)$  becomes reduced along the viscous flow, we can thus conclude that the centrifugal force is the primary cause of shock formation. When synchrotron cooling is effective in an inviscid accretion flow, the shock location ( $x_s = 22.94$ ) again proceeds towards the horizon, as depicted by the vertical dotted line. In the pre-shock region, density and temperature are low and therefore the effect of cooling is negligible (see below). The situation is completely opposite in the post-shock region and cooling reduces the post-shock pressure, causing the shock to move forward further. This indicates that thermal pressure is also no less important in determining the final shock location. In a generalized accretion flow, where both viscosity and cooling are present, the shock location is predicted at  $x_s = 18.62$  for the same set of input parameters as above, as denoted by the vertical dot-dashed line. In this particular case, the shock front is shifted significantly because of the combined effects of viscosity and cooling. When the mass loss from the viscous disc (Chattopadhyay & Das 2007) is considered, the shock is seen to form even closer to the black hole, as some part of the accreted matter is ejected as outflows, which reduces the post-shock pressure drastically.

Fig. 5(a) plots the logarithmic proton temperature ( $T = \mu m_p a^2 / \gamma k_B$ ) of a weakly viscous flow as a function of the radial distance for the same set of input parameters as in Fig. 4 with  $\beta = 0.0236$ . Clearly, Fig. 5(a) indicates that the post-shock temperature is much higher compared to the pre-shock temperature. This is because shock compresses the flow and makes it hotter. In particular, at the shock, the flow temperature rises sharply, as the kinetic energy of the flow is converted to thermal energy there. Fig. 5(b) shows how the total synchrotron loss (in logarithmic scale with geometric units)



**Figure 4.** Plot of Mach number with logarithmic radial distance. Flows with the same energy  $\mathcal{E}_{\text{inj}} = 3.3663 \times 10^{-3}$  and angular momentum  $\lambda_{\text{inj}} = 1.725$  at the outer edge  $x_{\text{inj}} = 145$  are injected with different dissipation parameters. The dissipation parameters are marked in the figure. The corresponding shock locations are indicated by the vertical lines:  $x_s = 25.99$  (solid),  $x_s = 20.6$  (dashed),  $x_s = 22.94$  (dotted) and  $x_s = 18.62$  (dot-dashed).

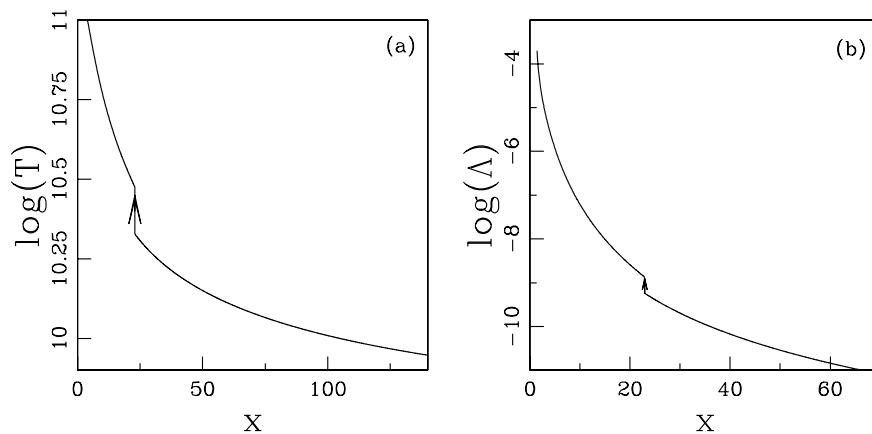


**Figure 5.** The variation of (a) flow temperature and (b) total synchrotron loss (in geometric units) with radial distance.

varies with the radial distance for the same set of flow parameters as in Fig. 5(a). The net energy loss is negligible in the pre-shock region while it increases significantly as the post-shock flow is advected towards the black hole.

Fig. 6(a) compares the shock locations as a function of the cooling parameter  $\beta$  for different values of angular momentum  $\lambda_{\text{inj}}$ . In all cases, the matter is injected at the outer edge of the disc  $x_{\text{inj}} = 145$ . The solid curve is for  $\lambda_{\text{inj}} = 1.7$  and the dotted and dashed curves are for  $\lambda_{\text{inj}} = 1.725$  and  $\lambda_{\text{inj}} = 1.75$ , respectively. The corresponding local energies at the injection point are  $\mathcal{E}_{\text{inj}} = 2.5156 \times 10^{-3}$  (solid line),  $3.3663 \times 10^{-3}$  (dotted line) and  $4.3474 \times 10^{-3}$  (dashed line).

This example shows that stable shocks can form for a wide range of cooling parameters. For a given local energy and angular momentum of the flow at the injection point, the shock location decreases with the increase of the cooling parameter as flow loses energy as it accretes. When cooling is above its critical value ( $\beta > \beta_{\text{cs}}$ ), shock ceases to exist as the RHCs are not satisfied there. An important point to note is that the shock forms at larger radii for higher angular momentum as the centrifugal barrier becomes stronger with angular momentum.

It is useful to study the density distribution across the shock as cooling processes as well as emergent radiation from the disc are

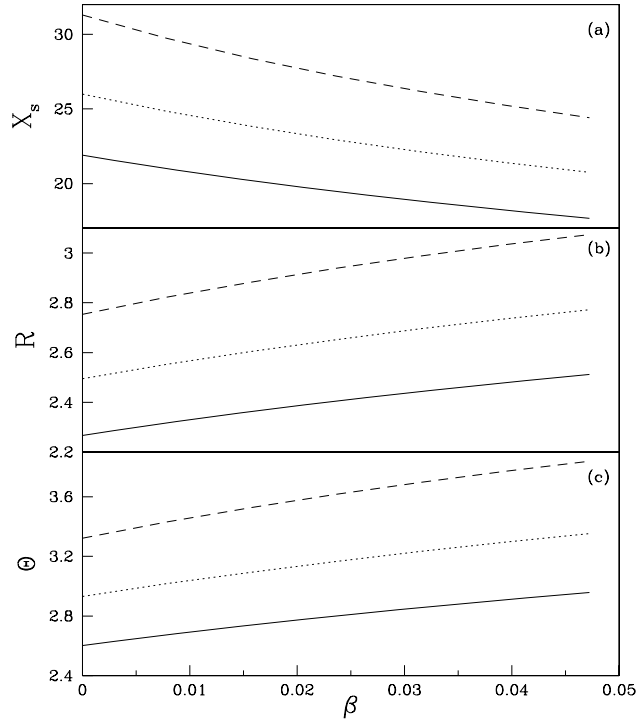


**Figure 6.** (a) Variation of shock location with cooling factor when flows with identical angular momentum and energy are injected from a fixed outer boundary. Solid, dotted and dashed curves are drawn for flow with angular momentum  $\lambda_{\text{in}} = 1.7, 1.725$  and  $1.75$ , respectively. Shock forms further for higher angular momentum flow suggests that shocks are mainly centrifugally driven. In all cases, the shock moves closer to the black hole as the cooling factor is increased. (b) Variation of compression ratio ( $R = \Sigma_+/\Sigma_-$ ) with cooling factor for the same set of parameters as in (a). Subscripts ‘+’ and ‘-’ refer to quantities before and after shock. The compression ratio monotonically increases in all cases as the cooling factor is increased. (c) Variation of shock strength ( $\Theta = M_-/M_+$ ) with cooling factor for the same set of parameters as in (a). The shock strength gradually increases in all cases as the cooling factor is increased.

strongly dependent on it (Chakrabarti & Mandal 2006). For this, we compute the compression ratio ( $R$ ), which is defined as the ratio of the vertical averaged post-shock density to the pre-shock density. As an example, in Fig. 6(b), we show the variation of compression ratio with the cooling parameter for the same set of flow parameters as in Fig. 6(a). For a given set of local energy and angular momentum of the flow, the compression ratio  $R$  increases monotonically with the cooling parameter. In a convergent accretion flow, the shock is pushed inwards when cooling is enhanced. This causes more compression in the post-shock region. There is a cut-off at a critical cooling limit as shock disappears there.

In our further study of shock properties, in Fig. 6(c), we draw the variation of the shock strength ( $\Theta$ ) with the cooling parameter. The shock strength is defined as the ratio of the pre-shock Mach number to the post-shock Mach number, and it determines the temperature jump at the shock. Here, we use the same set of initial parameters as in Fig. 6(a). In the dissipation-free limit, the strength of the shock is weak and it becomes stronger as the cooling parameter is increased.

## 5.2 General behaviour of shocks

So far, we have only studied the properties of shock waves when matter is injected from a fixed outer edge of the disc. In reality, global

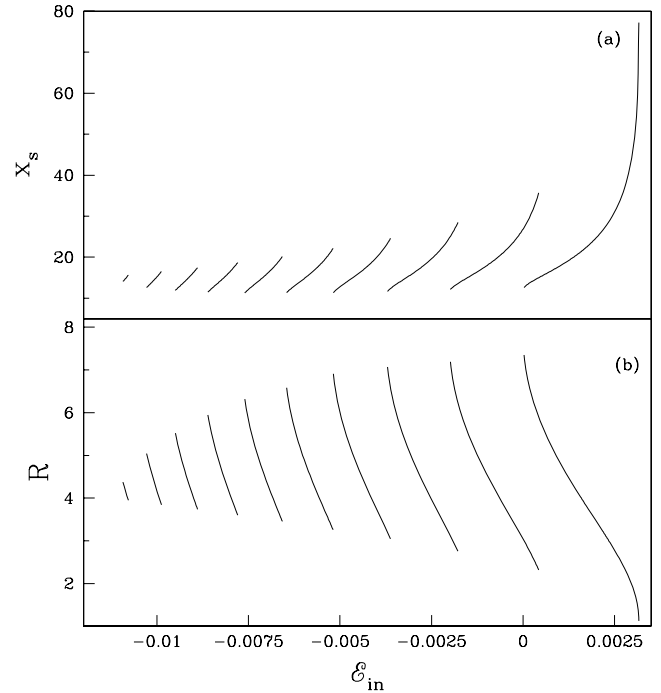


**Figure 7.** (a) Variation of shock location with flow energy at the inner sonic point. The different curves are drawn for different cooling factors. The rightmost curve is drawn for dissipation-free flow. As dissipation increases ( $\Delta\beta = 0.016$ ), shock forms at a closer distance. (b) Variation of compression ratio as a function of flow energy at the inner sonic point and the cooling factor. The flow parameters are same as in (a). The compression ratio decreases at both higher and lower ends as the cooling is enhanced.

solutions that contain shock waves are not isolated solutions, but are present in a large range of flow parameters. We continue our study of shock properties for a wide range of flow parameters. Fig. 7(a) shows the shock location ( $x_s$ ) as a function of specific energy at the inner sonic point  $\mathcal{E}_{\text{in}}$ . Different curves are drawn for a set of cooling parameters starting from  $\beta = 0.0$  (rightmost) to  $0.144$  (leftmost) with an interval  $\Delta\beta = 0.016$ . Here, the angular momentum at the inner sonic point is chosen as  $\lambda_{\text{in}} = 1.75$ . Notice that shock forms only for a particular range of  $\mathcal{E}_{\text{in}}$  and in the weak cooling limit, the shock location varies widely (in the range  $10\text{--}80 r_g$  in this particular set of parameters). At a higher cooling parameter  $\beta$ , shocks form at closer radii and the range of shock locations gradually shrinks. In particular, the upper limit of the shock locations proceeds more rapidly towards the black hole horizon with the increase of cooling parameter. When  $\beta > \beta_{\text{cs}}$  is reached, accreting flow fails to satisfy the RHC and the shock disappears. Shocks can even form at negative energies at the inner sonic point (in general, the flow is supposed to have positive energy at the shock). This indicates that as a result of cooling, flow loses a significant amount of energy while falling into the black hole.

Fig. 7(b) plots the variation of the compression ratio with  $\mathcal{E}_{\text{in}}$  for the same set of initial flow parameters used in Fig. 7(a). Each individual curve is obtained for a given cooling parameter ranging from  $\beta = 0.0$  (rightmost) to  $\beta = 0.144$  at intervals of  $\Delta\beta = 0.016$ . The strongest shocks ( $R \rightarrow 7$ ) form only in the weak cooling limit. Fig. 7(b) clearly shows that the upper and lower limits of the compression ratio monotonically decrease for the gradual increase of the cooling parameter, and finally compression merges to the intermediate value ( $R \sim 4$ , a measure of strong shock; see Das et al.

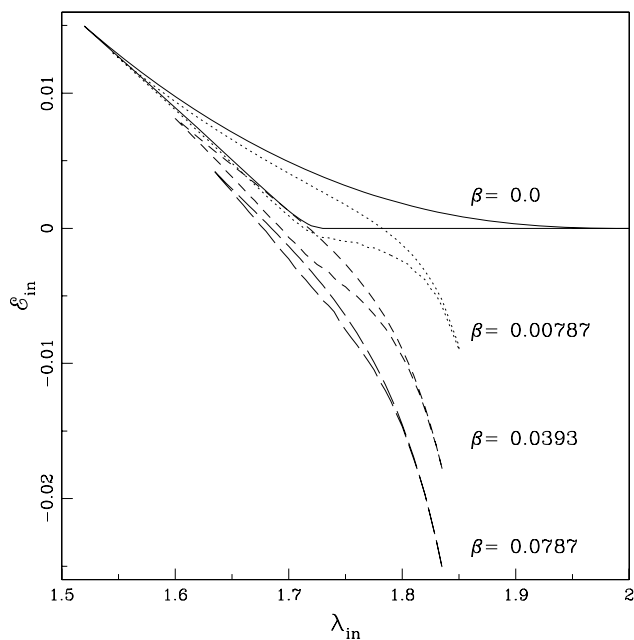


**Figure 8.** Modification of parameter space for standing shock as a function of cooling parameter. The parameter space shrinks with the increase of the cooling factor.

2001a and references therein) up to a critical cooling limit beyond which shock does not form. Thus, strong shocks are formed for a large range of cooling parameters, and outflow and jet are obviously expected to be produced in the presence of synchrotron cooling.

## 6 PARAMETER SPACE FOR SHOCK

In Fig. 8, we redraw the parameter space as shown in Fig. 2, but consider the formation of a standing shock only in a cooling dominated flow. The parameter space is expected to be modified with the increase of the cooling parameter. We identify the modified regions of the parameter space for stationary shock using various cooling parameters. The cooling parameters are shown in the figure. For  $\beta = 0.0$ , the region bounded by the solid curve identically merges with that of Chakrabarti (1989). At a higher cooling parameter, the effective region of the parameter space for a standing shock is reduced in both the higher and lower angular momentum sides, and it is also shifted to a negative energy region. Beyond a critical cooling limit, this region disappears completely.

We continue our study of parameter space in the energy–angular momentum ( $\mathcal{E}_{in}, \lambda_{in}$ ) plane according to the accretion flow topologies for  $\beta = 0.00787$  in the weak viscosity limit. The boundary denoted by the solid curve in Fig. 9 identifies the region of the parameter space for closed topologies passing through the inner sonic point (Fig. 1). Further subdivisions of parameter space are marked by dashed and dotted curves, depending on the behaviour of the solution topologies. Accretion topologies with parameters chosen from different regions of the parameter space are presented in the small boxes at the bottom left of Fig. 9. In each small box, we plot the variation of Mach number as a function of logarithmic radial distance. Flows with parameters from the region  $ABD$  possess multiple sonic points. In particular, when the flow parameters fall in the region  $ABC$  separated by the dashed boundary, RHCs are satisfied. The accretion solution of this type is drawn in the box labelled S. However, for flows with parameters from the rest of the  $ABD$  region, RHCs are not satisfied, but the entropy of the flow

at the inner sonic point continues to be higher compared to that at the outer sonic point. In this case, the shock starts oscillating, causing a periodic breathing of the post-shock region (Ryu et al. 1997). The box marked OS shows an accretion solution having oscillating shock. For higher cooling, we obtain a new solution topology, as shown in the box labelled CIM, as seen in Das & Chakrabarti (2004). We draw this solution with a dotted curve as it is obtained for a higher cooling parameter. This multivalued solution is expected to be unstable and may cause a non-steady accretion. The accretion solution with parameters from the I region of the parameter space is drawn in the box labelled I. This accretion solution immediately passes through the inner sonic point before entering into the black hole. The solution inside the box labelled O represents an accretion flow that passes through the outer sonic point only. The box marked CI shows a closed accretion solution passing through the inner sonic point. This type of solution does not extend to the outer edge to join smoothly with any Keplerian disc, and flow is expected to be unstable. When dissipation is significantly increased, the closed topology of CI opens up (Fig. 1) and then flow can join with the Keplerian disc.

Fig. 10 shows the comparative study of the parameter space for standing shocks in different dissipation limits. The dissipation parameters are marked. The solid boundary separates the parameter space for standing shock in the non-dissipative accretion flow (Chakrabarti 1989). When the viscosity is included, the effective region of the parameter space for standing shock reduces and shifts towards higher energy and lower angular momentum regime (Chakrabarti & Das 2004). The region bounded by the dot-dashed curve is obtained for standing shocks in viscous flow. However, for a cooling dominated inviscid accretion flow the parameter space for standing shock shrinks at both ends of the angular momentum (lower and higher) and moves to the lower energy sides (present paper). This parameter space is shown by the dashed curve. When viscosity and cooling are both present, the parameter space for shock settles at an intermediate region (shaded part). This indicates that viscosity and synchrotron cooling act in opposite ways to decide the shock parameter space. However, they behave similarly while controlling the dynamics of the shock waves (Fig. 4).

## 7 CRITICAL COOLING PARAMETER

In the above discussion, we have already mentioned that the global behaviour of the cooling dominated accretion flow changes when the cooling parameter exceeds its critical value. In particular, there are two critical cooling parameters: the first identifies a boundary that separates the closed topologies from the open topologies passing through the inner sonic point; the second is obtained at the region of the closed solutions based on the criteria of whether a standing shock is formed or not. These critical cooling parameters of course depend greatly on the inflow parameters. Fig. 11 shows a plot of the critical cooling parameters versus angular momentum at the inner sonic point. Different regions are marked. The figure shows that closed topologies as well as shocks are formed at the lower and higher angular momentum sides for smaller cooling parameters. As the cooling parameter is increased, the shock forms only somewhere at the intermediate angular momentum domain, which is consistent with our earlier discussion.

## 8 CONCLUDING REMARKS

In this paper, we have presented the properties of viscous accretion flows around a stellar-mass black hole in presence of synchrotron

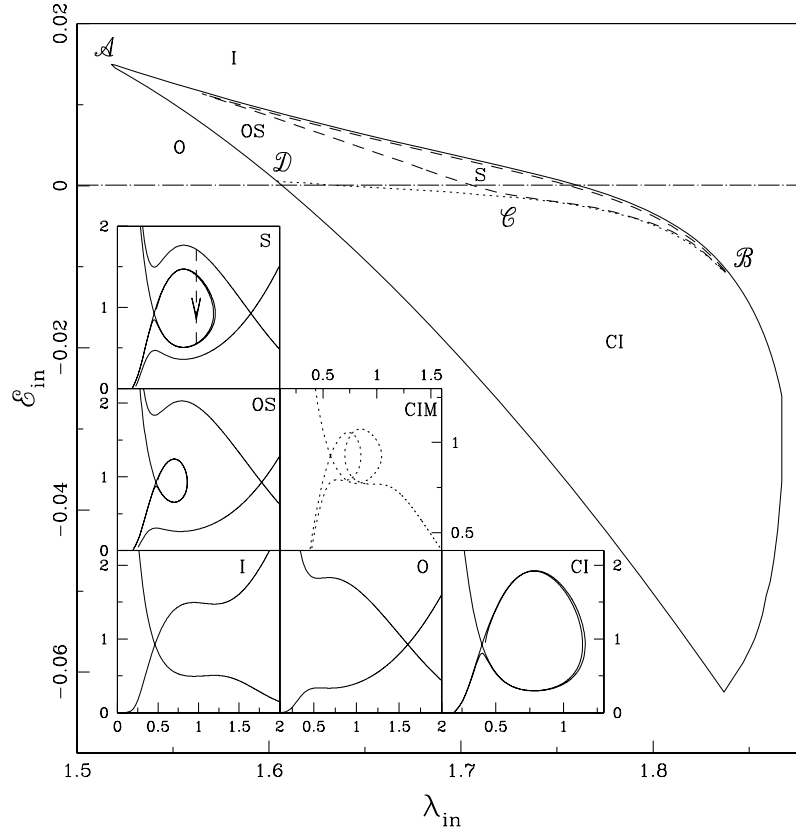


**Figure 9.** Division of parameter space in the  $\mathcal{E}_{\text{in}}$ ,  $\lambda_{\text{in}}$  plane according to the topologies. Accretion solutions with parameters taken from different parts of the parameter space are shown in the insets.

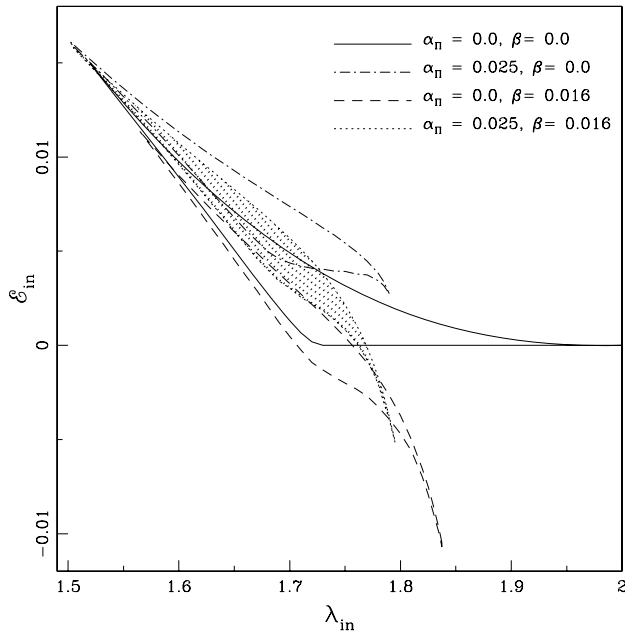


**Figure 10.** Region of the parameter space for standing shock for different dissipation parameters. Dissipation parameters are marked in the figure.

cooling. In a realistic accretion flow, the energy loss because of radiation is not negligible and it has a significant effect on the dynamical structure of the flow, as we show here. This will also alter the emitted spectrum and luminosity.

Efforts have been made previously to study the properties of viscous transonic flow in the cooling free limit (Chakrabarti 1990; Chakrabarti & Das 2004) and/or cooling has been considered in an approximate way (Chakrabarti 1996b). No attempts have been made to study a complete accretion solution, which may contain shocks in the presence of synchrotron cooling. Here, we have obtained a complete set of global solutions. We have shown that for a large region of the parameter space a transonic flow can have shock waves when viscosity as well as synchrotron cooling is very high. We find that the shock locations may vary from around 10 Schwarzschild radii to several tens of Schwarzschild radii, depending on the inflow parameters. We have shown that standing shocks, where a significant amount of conversion from kinetic energy to thermal energy takes place, can form much closer to the black hole with the enhancement of dissipation. For higher viscosity, flow transports angular momentum more and more, as the flow moves inward, and at the same time it tends to heat the flow. This causes the centrifugal pressure to be much lower at the post-shock region although the post-shock thermal pressure is higher. When the viscosity parameter is increased, shock forms closer to the black hole horizon, indicating that perhaps shocks are centrifugal pressure supported. However, synchrotron photons generated by the stochastic/random magnetic field can cool down the flow and, in addition, the flow angular momentum distribution remains insensitive to it (equation 3). As the synchrotron cooling is increased, the post-shock flow is cooled down more efficiently and the thermal pressure in this region reduces significantly. This causes the shock to move inwards to maintain pressure balance (thermal plus ram) across it. Thus, viscosity and cooling play a similar role as far as the dynamic properties of the shock are concerned. However,

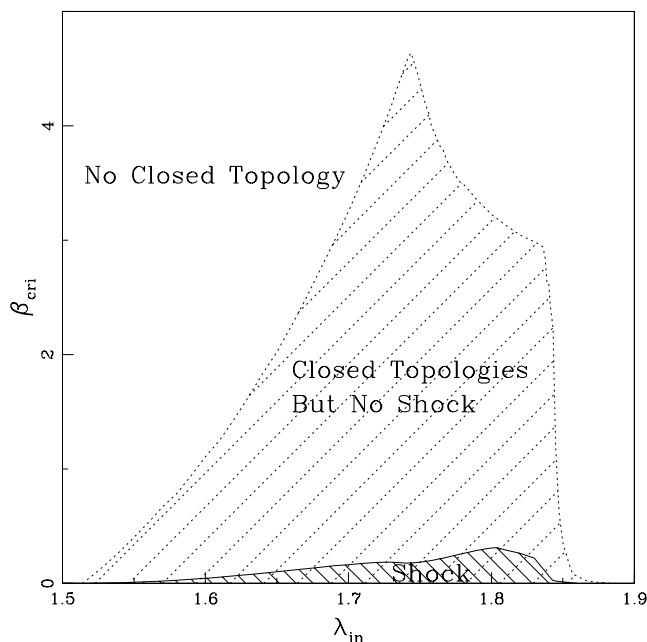


**Figure 11.** Variation of the critical cooling parameter as a function of angular momentum at the inner sonic point. The region outside the dotted curve allows solutions with open topologies and the region shaded by solid lines separates the standing shock solutions from the oscillating shock.

cooling cannot completely nullify the effect of viscous heating, as dissipation processes depend differently on the flow variables.

We obtain the parameter space for standing shock waves as a function of cooling parameter and we find that the effective region of the parameter space shrinks as the cooling parameter is enhanced. We also identify the region of the parameter space where standing shock conditions (RHCs) are not favourable but accreting solutions that have two saddle-type sonic points are present. These solutions generally exhibit non-steady shocks (Ryu et al. 1997) which could even form when cooling is very high. Moreover, the possibility of shock formation decreases with an increasing cooling parameter, and when the cooling parameter is increased beyond a critical value, the shocks disappear (Fig. 11). We also find that viscosity and synchrotron cooling induce completely opposite effects in deciding the parameter space for stationary shock waves. Indeed, it is clear that cooling affects the dynamics of the accretion flow as well as the shock parameter space quite significantly. Therefore, the cooling free assumption (Gu & Lu 2004) is perhaps too simplistic in a general transonic accretion flow.

We have argued that black hole accretion models may need to include shock waves as they provide a complete explanation of the observed steady state, as well as time-dependent behaviour (Chakrabarti & Titarchuk 1995; Ryu et al. 1997). In particular, as cooling is increased, post-shock energy decreases and shock location is reduced. In addition, earlier studies (Chakrabarti & Manickam 2000; Ryu et al. 1997) have shown that QPOs of hard radiation from black holes is proportional to the infall time, and therefore QPO frequency increases with the enhancement of the cooling parameter. Observational findings do support this view that for higher accretion rate, QPO frequency increases. Therefore, possibly shocks may be an active ingredient in the accretion flow.

In this paper, we have shown that for a given set of flow parameters there are two critical cooling parameters that separate the parameter space into three regions (Fig. 11). In the first region, flow passes

through a single X-type sonic point. In the second region, flow has multiple sonic points but Rankine–Hugoniot relations are not favourable anywhere, while in the third region Rankine–Hugoniot relations are satisfied and standing shocks form.

An important point we need to discuss is that because the basic physics of advective flows is similar around a neutron star (differing from a black hole solution only in inner boundary conditions), the present formalism could be applicable, although the boundary of the neutron star, where half of the binding energy could be released, may be more luminous than that of a black hole.

In our calculation, we have made some approximations; for example, we consider a stochastic magnetic field instead of a large-scale field. We ignore the effect of radiation pressure. Also, we assume a fixed polytropic index rather than computing it self-consistently. We use the Paczyński–Wiita pseudo-potential (Paczyński & Wiita 1980) to describe the space–time geometry around a Schwarzschild black hole. However, we believe that our basic conclusion will not be affected qualitatively by these approximations. More generalized calculations around a rotating black hole are beyond the scope of this paper and will be reported elsewhere.

## ACKNOWLEDGMENTS

The author is thankful to Sandip K. Chakrabarti for his useful suggestions and discussions. He also thanks I. Chattopadhyay for suggesting improvements for the manuscript. This work was supported by KOSEF through the Astrophysical Research Center for the Structure and Evolution of the Cosmos (ARCSEC).

## REFERENCES

- Abramowicz M. A., Kato S., 1989, *ApJ*, 336, 304  
 Abramowitz M., Stegun I. A., 1970, *Handbook of Mathematical Functions*. Dover, New York  
 Afshordi N., Paczyński B., 2003, *ApJ*, 592, 354  
 Chakrabarti S. K., 1989, *ApJ*, 347, 365  
 Chakrabarti S. K., 1990, *Theory of Transonic Astrophysical Flows*. World Scientific, Singapore  
 Chakrabarti S. K., 1996a, *Phys. Rep.*, 266, 229  
 Chakrabarti S. K., 1996b, *ApJ*, 464, 664  
 Chakrabarti S. K., Das S., 2004, *MNRAS*, 349, 649  
 Chakrabarti S. K., Mandal S., 2006, *ApJ*, 642, L49  
 Chakrabarti S. K., Manickam S. G., 2000, *ApJ*, 531, L41  
 Chakrabarti S. K., Molteni D., 1995, *MNRAS*, 417, 672  
 Chakrabarti S. K., Titarchuk L. G., 1995, *ApJ*, 455, 623  
 Chakrabarti S. K., Titarchuk L., Kazanus D., Ebisawa K., 1996, *A&A*, 120, 163  
 Chakrabarti S. K., Acharyya K., Molteni D., 2004, *A&A*, 421, 1  
 Chattopadhyay I., Chakrabarti S. K., 2000, *Int. J. Mod. Phys. D*, 9, 117  
 Chattopadhyay I., Chakrabarti S. K., 2002, *MNRAS*, 333, 454  
 Chattopadhyay I., Das S., 2007, *New Astron.*, in press (doi: 10.1016/j.newast.2007.01.006)  
 Chaudhury S., Ray A. K., Das T. K., 2006, *MNRAS*, 373, 146  
 Das S., Chakrabarti S. K., 2004, *Int. J. Mod. Phys. D*, 13, 1955  
 Das S., Chattopadhyay I., Nandi, A., Chakrabarti S. K., 2001a, *A&A*, 379, 683  
 Das S., Chattopadhyay I., Chakrabarti S. K., 2001b, *ApJ*, 557, 983  
 Dhawan V., Mirabel I. F., Rodriguez L. F., 2000, *ApJ*, 543, 373  
 Ebisawa K., Titarchuk L., Chakrabarti S. K., 1996, *PASJ*, 48, 59  
 Fender R. P., Pooley G. G., Durouchoux P., Tilanus R. P. J., Brocksopp C., 2000, *MNRAS*, 312, 853  
 Ferrari A., Trussoni E., Rosner R., Tsinganos K., 1985, *ApJ*, 294, 397  
 Fukumura K., Tsuruta S., 2004, *ApJ*, 611, 964  
 Gu W.-M., Foglizzo T., 2003, *A&A*, 409, 1  
 Gu W. M., Lu J. F., 2004, *Chin. Phys. Lett.*, 21, 2551  
 Landau L. D., Lifshitz E. D., 1959, *Fluid Mechanics*. Pergamon, New York

- Lanzafame G., Molteni D., Chakrabarti S. K., 1998, MNRAS, 299, 799  
Lightman A. P., Eardley D. M., 1974, ApJ, 187, 1  
Lu J. F., Yuan F., 1997, PASJ, 49, L525  
Mandal S., Chakrabarti S. K., 2005, A&A, 434, 839  
Matsumoto R., Kato S., Fukue J., Okazaki A. T., 1984, PASJ, 36, 7  
Molteni D., Sponholz H., Chakrabarti S. K., 1996, ApJ, 457, 805  
Molteni D., Toth G., Kuznetsov O. A., 1999, ApJ, 516, 411  
Muchotrzeb-Czerny B., 1986, Acta Astron., 36, 1  
Nobuta K., Hanawa T., 1994, PASJ, 46, 257  
Paczynski B., Wiita P. J., 1980, A&A, 88, 23  
Ryu D., Chakrabarti S. K., Molteni D., 1997, ApJ, 474, 378  
Shakura N. I., Sunyaev R. A., 1973, A&A, 24, 337  
Shapiro S. L., Teukolsky S. A., 1983, Black Holes, White Dwarfs and Neutron Stars: The Physics of Compact Objects. Wiley-Interscience, New York  
Smith D. M., Heindl W. A., Markwardt C. B., Swank J. H., 2001, ApJ, 554, L41  
Smith D. M., Heindl W. A., Swank J. H., 2002, ApJ, 569, 362  
Sunyaev R. A., Titarchuk L. G., 1985, A&A, 143, 374  
Yang R., Kafatos M., 1995, A&A, 295, 238

This paper has been typeset from a  $\text{\TeX}/\text{\LaTeX}$  file prepared by the author.